annalen der physik
www.ann-phys.org

Dielectric-Based Electromagnetically Induced Transparency Metamaterial in the Microwave Band

*Han-Qing Dong, Cheng-Jing Gao, and Hai-Feng Zhang**

An electromagnetically induced transparency metamaterial (EITM) based on dielectric resonators is presented in this paper, which consists of a cut wire (CW) and ten dielectric columns. Destructive interference between the CW, which is a branch of the microstrip line, and the dielectric resonators causes the EIT phenomenon. The simulation results show that the dielectric-based EITM designed can obtain a transmission peak of 0.938 at 2.17 GHz, and the two-oscillator model is utilized to verify the effectiveness of the structure. In addition, samples of the dielectric-based EITM are also fabricated and the effectiveness of the metamaterial is experimentally verified. The proposed metamaterial has several advantages, including high efficiency, low loss, a simple structure, and ease of manufacture, which has good prospects for application in the fields of electromagnetic switches, sensors, and nonlinear metamaterials.

1. Introduction

The electromagnetically induced transparency (EIT) effect is an optical phenomenon, which originally belonged to the atomic domain. The essence of the EIT phenomenon is that when the frequency of light matches the leap frequency of the corresponding atomic, quantum between light-atom excitation channels produces phase extinction interference, so that a very narrow transmission peak appears in the wide absorption band. The EIT effect drastically changes the refractive index of some materials that are opaque originally, making them transparent at a certain wavelength. This process produces a strong slow-light effect and enhances the nonlinear effect of the material, which enables them to be effectively applied to optical buffer[1,2] devices and refractive index sensing[3–5] and other fields.

It is worth noting that the realization of the EIT effect in atomic systems often requires harsh experimental conditions such as ultra-low temperature[6] and intense light pumping, which caused the practical value of the EIT effect to be greatly reduced. The emergence of metamaterials effectively resolved this issue. Utilizing logical structural design and material selection, scholars are now able to achieve effective transmission of the EIT in the microwave,[7–9] infrared, terahertz,[10,11] and other frequency bands under conventional experimental conditions, and the related optical instrumentation manufacturing technology is gradually maturing.

The artificial structural units are arranged in different topologies that constitute the metamaterials. Metamaterials can actualize innovative physical features and functions that natural materials cannot realize and access the value domain space that natural media cannot access. Therefore, metamaterials have received extensive attention and research from scholars at home and abroad. From the point of view of the structure of the material, metamaterials are generally composed of a number of artificial electromagnetic structural units with sizes in the subwavelength order, so the interactions between structural units can be neglected. Through the selection of suitable substrate and surface materials and the rational design of their relevant structural parameters, the processed metamaterials are often able to produce resonant coupling with electromagnetic waves in different frequency bands.[12] Therefore, metamaterials can realize some electromagnetic properties that are difficult to achieve under ordinary natural materials or usual conditions, such as negative refractive index,[13,14] anti-reflective increase in permeability, broadband absorbers,[15–17] photonic bandgap crystals, electromagnetic-induced transparency[18,19] effect. Now, scholars have made a lot of progress in the field of electromagnetically induced transparent metamaterials (EITMs). In 2013, Han et al.[20] realized the EIT phenomenon through a self-asymmetric planar metamaterial. The transmission bandwidth can be varied by changing the depth of the structure. Hu et al.[21] demonstrated an EITM consisting of two metal strips with different lengths and a double split-ring resonator, in 2015. The single-band and double-band EIT phenomena were achieved in the microwave region by changing the lengths of the two metal strips. In 2018, Bagci et al.[22] used a square resonator as the bright mode and four split ring resonators (SRRs) as the quasi-dark mode. The two modes are coupled with each other to realize the EIT phenomenon. In addition, the transmission bandwidth and group time delay can be changed by controlling the incidence angle of electromagnetic waves.

In recent years, in the investigation of microstrip-line-based EITMs, metal resonators are frequently employed. In 2014, Zhu et al.[23] proposed that two metal-based detuned SRRS which near the microstrip line can couple with each other to produce the EIT

H.-Q. Dong, C.-J. Gao, H.-F. Zhang
College of Electronic and Optical Engineering and the College of Flexible Electronics (Future Technology)
Nanjing University of Posts and Telecommunications (NJUPT)
Nanjing 210023, P. R. China
E-mail: hanlor@njupt.edu.cn

The ORCID identification number(s) for the author(s) of this article can be found under https://doi.org/10.1002/andp.202300192

DOI: 10.1002/andp.202300192

Table 1. The comparison between the published reports and the proposed EITM.

References	Frequency regime	Peak	Metal Resonators	Dielectric Resonators	Transmission peak over 0.9
[26]	465–482 THz	473.2 THz	×	√	×
[27]	8.06–8.4 THz	8.25 THz	×	√	√
[28]	15–15.8 GHz	15.4 GHz	√	×	×
[22]	4.56–5.85 GHz	5.04 GHz	√	×	×
This work	1.12–2.99 GHz	2.17 GHz	√	√	√

effect. If the geometrical parameters of the SRRs are changed, the resonant frequency, transmission amplitude, and linewidth of the transparent window are also changed. In 2018, Amin et al.[24] devised a new guided wave resonator that consists of microstrip open stubs. The EIT phenomenon is caused by two closely connected microstrip open stubs being coupled together. In addition, when a third stub is added, a new EIT band is created. By adjusting the capacitance between adjacent stubs, the EIT phase response can be changed dynamically.

However, due to the ohmic loss of metal resonators, it is difficult for these typical structures to achieve efficient transmission, thus limiting the application of EITMs in ultra-low loss devices is discussed. Therefore, the research on dielectric-based metamaterials has increased recently. Dielectric materials usually have high dielectric constants, which may better prevent the scattering absorption and energy loss brought by metallic materials, thus significantly improving the transmission efficiency. This not only provides both a simpler and more efficient way to achieve ultra-low loss devices in the high-frequency range but also further promotes the development and application of the EITMs.[25] To reduce the impact of the ohmic loss, the combination of metal and dielectric resonators is used in this work.

In this paper, a dielectric-based EITM with high transmission efficiency is designed, which consists of a metallic cut wire (CW) as the bright mode and ten cylindrical-shaped dielectric resonators as the dark mode. The CW is directly connected to the microstrip transmission line, which is excited by the input wave, while the dielectric resonators are almost unexcited. The two are coupled to each other and produce phase extinction interference which results in the EIT phenomenon. By the simulation of this dielectric-based metamaterial, a transparent window can be obtained at 2.17 GHz and the transmission peak can reach 0.983. In addition, to confirm the validity of the dielectric EITM, the corresponding experimental samples were made. Linh et al.[26] proposed a silicon-based EITM. This metamaterial all uses dielectric resonators that also has great application prospects in the field of slow light devices. Zhu et al.[27] presented an EITM consisting of two-different sized bi-air-hole cubes (BCs). The EIT phenomenon occurs in the terahertz band, and it has high transmission peaks. Jin et al.[28] proposed an EITM that consists of two SRRs. And the control of the EIT phenomenon can be achieved by adjusting the incidence angle. Bagci et al.[22] devised a metamaterial consisting of a square ring resonator and four SRRs. Narrowband and broadband EIT phenomena were achieved by varying the design. Compared with these EITMs, our proposed structure combines the metal resonator with dielectric resonators and achieves high-efficiency transmission based on the microstrip line, as illustrated in **Table 1**. The efficient EIT structure proposed in this paper has universal applicability. It also has promising applications in the fields of electromagnetic switches, sensors, and nonlinear optics.

2. Modeling and Simulation

The dielectric-based EITM designed in this paper contains only one unit. The structure of the metamaterial is shown in **Figure 1**, which is composed of three parts: dielectric substrate, metal CW and dielectric resonators. The CW is directly connected to the microstrip line, which is a branch of the microstrip line. The dielectric-based metamaterial is constructed on FR4 substrate (relative permittivity is 4.4) and the dielectric resonators are made of ceramic (relative permittivity is 40, quality factor is 60 000 and relative permeability is 1). The material for the metal CW and the microstrip line is copper with a thickness of 0.035 mm and an electric conductivity of 57 142 857 S m^{-1}. The width of the microstrip line and CW are chosen to be 2 mm. The other parameters of the dielectric-based EITM are listed in **Table 2**. The microstrip line uses traditional PCB board fabrication methods,[29] while the dielectric resonators use alumina fabrication methods. All numerical simulations in this paper are obtained by High Frequency Structure Simulator (HFSS). Since HFSS uses a mesh-split finite element algorithm, before starting the calculations, an air box needs to be built in HFSS to create a microwave darkroom to simulate free space. It is also necessary to set the ports at both ends of the microstrip line, which are tiny rectangular patches. The length of both rectangular ports is 2.07 mm and their width is 2 mm. Signals can be injected into the structure through these two ports.

The CW as one branch of the microstrip line can be directly excited by the input wave and generates an asymmetric resonance at 1.55 GHz. The resonator that can be directly excited by input wave and produce a significant resonance is defined as the bright mode, so the CW can be seen as the bright mode of the EIT metamaterial, whose transmission spectrum can be seen in **Figure 2**a (blue curve). While only ten columnar dielectric resonators are placed near the microstrip wire, the transmission spectra are shown in Figure 2a (red curve). It can be seen that the ten dielectric resonators, which generate two weak symmetric resonances, are weakly excited at 1.07 and 3.27 GHz under the influence of the input wave.[30] Such resonators, which are hardly excited by the input wave, can be defined as the dark mode. Fano resonance is a resonant phenomenon with asymmetric line shapes that arises from the interference coupling between a narrow discrete resonance with a broad spectral line. A Fano resonance can be formed, when we place the bright and dark resonators near the microstrip line at the same time, the transmission spectrum

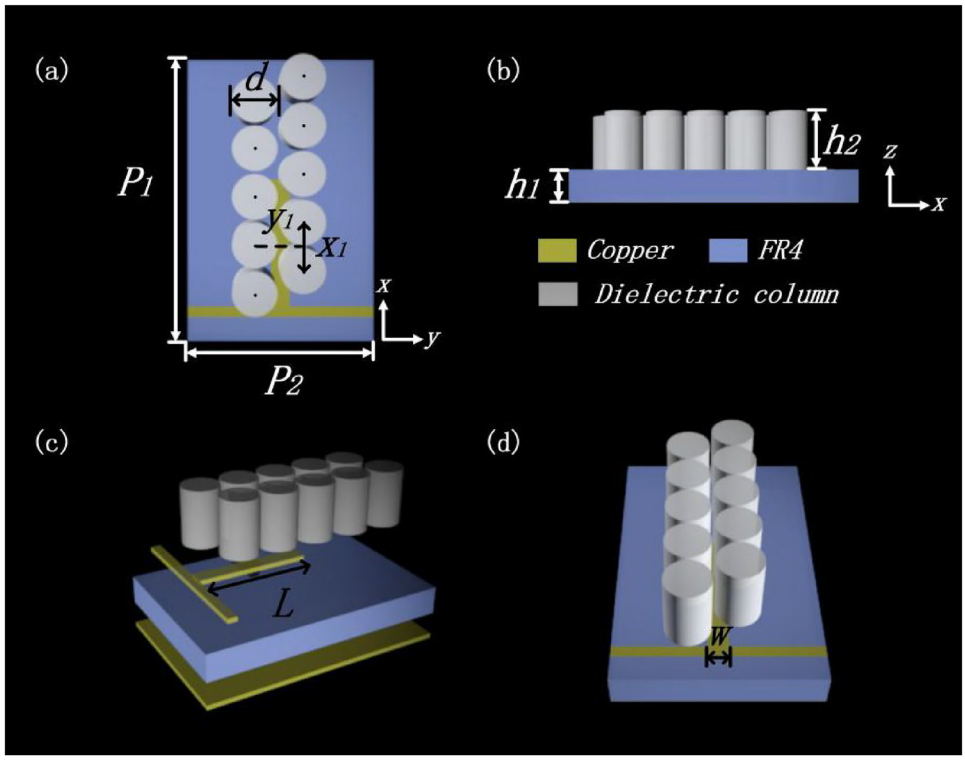

Figure 1. The schematic views of the metal-dielectric-based metamaterial, a) the top view, b) the side view, c) the separation schematic view, d) the 3D view.

Table 2. The detailed geometrical dimensions of the structure.

Parameters	P_1	P_2	d	w	L
Value (mm)	53	35	8	3.5	24
Parameters	h_1	h_2	x_1	y_1	
Value (mm)	2	10	8.5	8	

is shown in Figure 2b. A transparent window can be obtained at 2.17 GHz and the transmission peak can reach 0.983. The two transmission valleys are generated at 1.12 and 2.99 GHz with values of 0.008 and 0.041, respectively.

When considering the loss tangent of the FR4 substrate (the loss tangent is 0.02), the transmission spectrum is shown in **Figure 3**. It can be seen that the newly obtained transmission curve has changed very little compared to the original one.

Furthermore, the loss of this EITM is also calculated. The absorption of the EITM is revealed in **Figure 4**. The absorption values corresponding to the transmission peak and the two dips are 0.017, 0.034, and 0.100 respectively. In the frequency range of 1.12–2.99 GHz, absorption is below 0.1, so this EITM is very effective in reducing ohmic losses.

The distributions of the electric and magnetic fields at the three frequency points of 1.12, 2.17, and 2.99 GHz is displayed in **Figures 5** and **6**. From Figures 5 and 6, it can be seen that

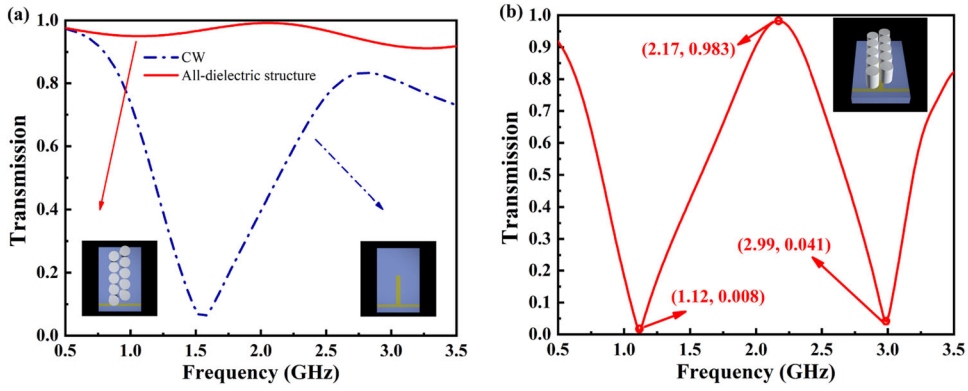

Figure 2. The transmission spectra of a) the CW (blue line) and the ten columns (red line), b) the metal-dielectric-based metamaterial.

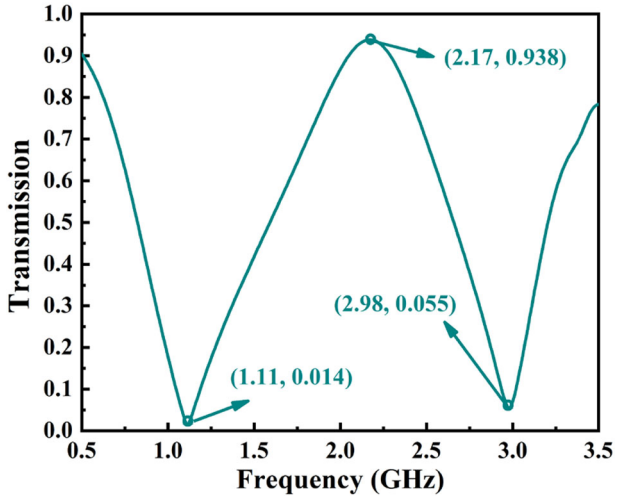

Figure 3. Transmission curve after considering the material loss.

the intensities of the electric and magnetic fields on CW are significantly stronger than those on the ten dielectric columns, and the intensities of the electric and magnetic fields on the dielectric columns are weak overall. As presented in Figure 5 the distributions of the electric field on the CW at 1.12 GHz, and 2.99 GHz are relatively strong and concentrate on the upper side (the side away from the microstrip line), and the distribution of the electric field on the CW at 2.17 GHz is relatively weak. For the ten dielectric columns, the regularity of the distribution of the electric field is similar to that on the CW. The electric field intensity at 2.17 GHz is the weakest among the three frequency points. As can be seen from Figure 6, the distributions of the magnetic field on both the CW and dielectric columns are the strongest at 2.17 GHz, and the weakest magnetic field strength is found at 2.99 GHz of the CW, while that of the dielectric columns are the weakest at 1.12 GHz. The CW is directly connected to the microstrip line, which is excited by the input wave. Therefore, strong electric and magnetic resonances are generated. The CW is considered to be a bright mode because it can directly derive

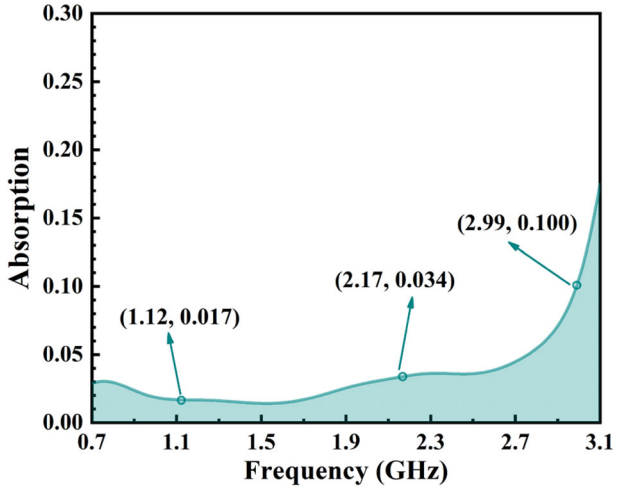

Figure 4. The absorption of the EITM.

energy from the input wave. Meanwhile, the dielectric columns can be excited and generate weak MIE resonance, so it is regarded as the dark mode. The bright and dark modes are coupled to each other to produce destructive interference, which is the reason for the EIT phenomenon, and a transmission peak appeared at 2.17 GHz. The bright mode coupling part of the energy to the dark mode, so that the Mie resonance of the dark mode is enhanced.[31] At the two transmission zeros, the energy coupling to the resonators is primarily due to electric field coupling, while at the transmission peaks, the energy coupling to the resonators is primarily due to magnetic field coupling. Furthermore, it can be seen that the dielectric columns have higher energy in the vicinity of the centerline, because they not only couple with the CW, but also exhibit resonances between each other. The staggered arrangement of the dielectric columns allows the dielectric resonators to fully couple with each other, enhancing the resonances between the dielectric columns.

3. Explanation of Principle

The three-level atomic system is often used to explain the EIT phenomenon. As presented in **Figure 7**, in the three-level atomic system, $|1>$ is the ground state energy level, $|2>$ is the metastable state energy level, and the common excited state energy level is $|3>$. Ω_1 and Ω_2 represent the phases of transition. The atoms absorb the energy and jump from $|1>$ to $|3>$ when a strong pumping beam is supplied, creating a transition channel.[32] Similarly, when a probing light is provided, a transition channel is generated from the metastable energy level $|2>$ to the excited energy level $|3>$. The EIT phenomenon is caused by the destructive interference between the two transition channels. The transition from $|1>$ to $|3>$ corresponds to the CW (bright mode) in the structure of this paper, and the transition from $|3>$ to $|2>$ corresponds to the dielectric columns (dark mode). Thus, under the action of the input wave, the CW can combine with the dielectric columns and produce a transparent peak at 2.17 GHz.

To better understand the EIT phenomenon the model of the two-oscillator model is introduced. The dielectric columns (dark mode) of the metamaterial are equivalent to the oscillator, which is not excited by the external field, whereas the CW (bright mode) is analogous to the oscillator excited by an external field. The two oscillators satisfy Equations (1) and (2):[33]

$$\ddot{x}_1(t) + \gamma_1 \dot{x}_1(t) + \omega_0^2 x_1(t) + \Omega^2 x_2(t) = gE \tag{1}$$

$$\ddot{x}_2(t) + \gamma_2 \dot{x}_2(t) + (\omega_0 + \delta)^2 x_2(t) + \Omega^2 x_1(t) = 0 \tag{2}$$

The outer field $E = E_0 e^{i\omega t}$, ω_0 and $(\omega_0 + \delta)$ are the resonant frequencies of the bright resonator and the dark resonator.x_1, x_2 and γ_1, γ_2 are the amplitude and damping constants of the bright and dark modes. The coupling constant between the two oscillators is Ω. The expression for the variation of x_n with t is $x_n(t) = c_n e^{i\omega t}$ (n = 1,2), c_n can be expressed as:[34] $c_n = \frac{gE_0}{\omega_n^2 - \omega^2 + i\gamma_1 \omega}$. The approximation relation of $\omega_0^2 - \omega \approx -2\omega_0(\omega - \omega_0)$is used. We can obtain Equation (3):[31]

$$T = 1 - \mathrm{Re}\left[\frac{ig^2(\omega - \omega_0 - \delta + i\gamma_2/2)}{(\omega - \omega_0 + i\gamma_1/2)(\omega - \omega_0 - \delta + i\gamma_2/2) - \Omega^2/4}\right] \tag{3}$$

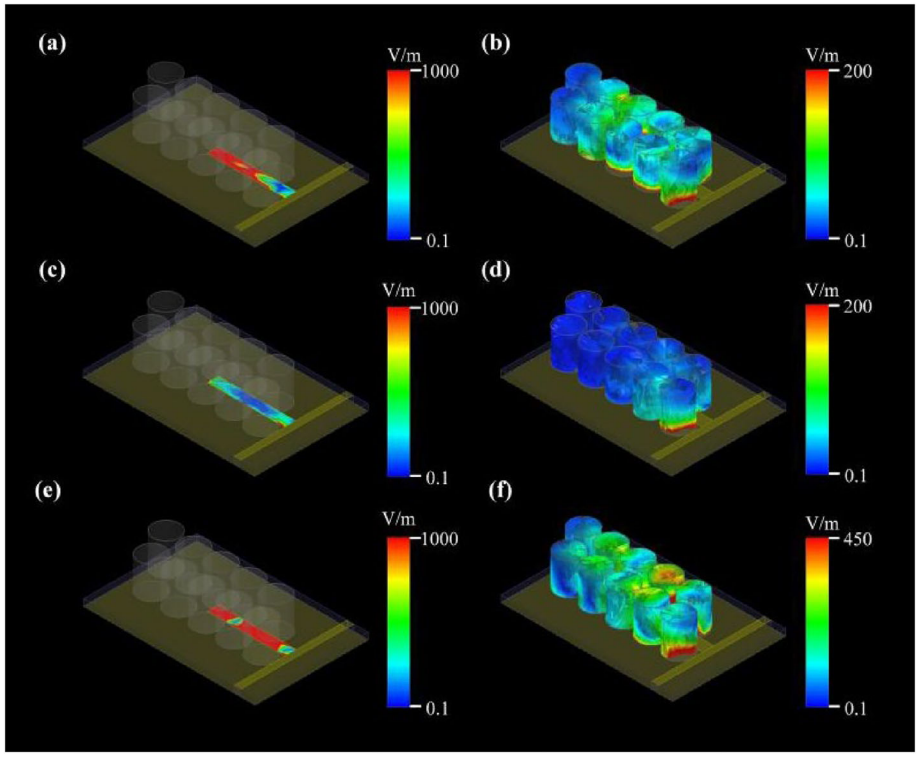

Figure 5. The distributions of the electric field at 1.12 GHz, 2.17 GHz and 2.99 GHz, a and b) the intensity of the electric field at 1.12 GHz of the CW and the dielectric columns, c and d) the intensity of the electric field at 2.17 GHz of the CW and the dielectric columns, e) and f) the intensity of the electric field at 2.99 GHz of the CW and the dielectric columns.

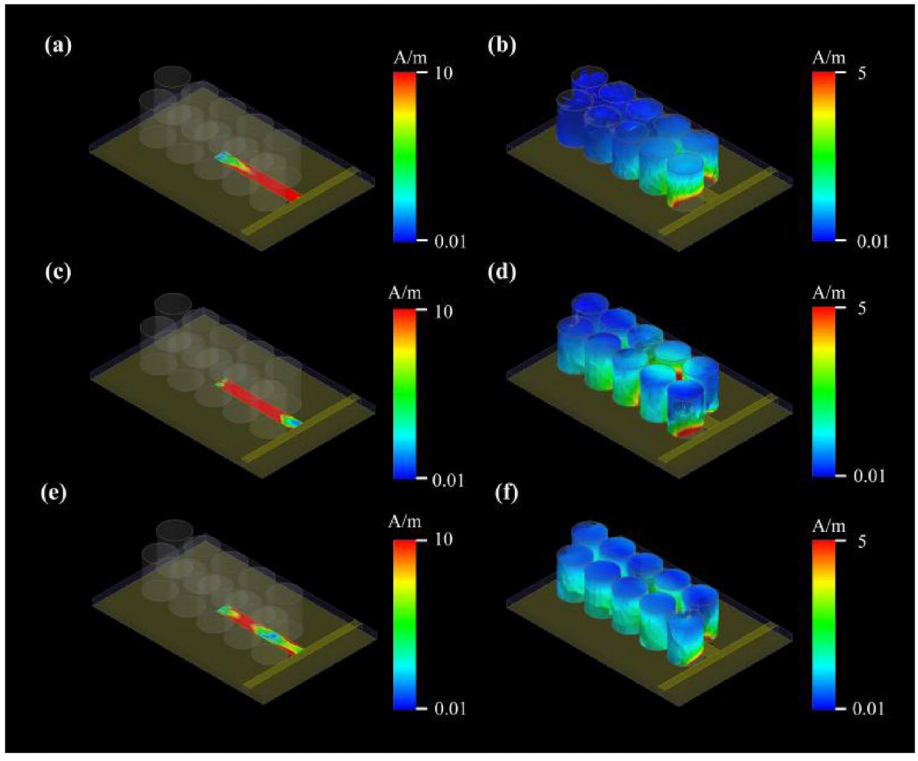

Figure 6. The distributions of the magnetic field at 1.12 GHz, 2.17 GHz and 2.99 GHz, a and b) the intensity of the magnetic field at 1.12 GHz of the CW and the dielectric columns, c and d) the intensity of the magnetic field at 2.17 GHz of the CW and the dielectric columns, e and f) the intensity of the magnetic field at 2.99 GHz of the CW and the dielectric columns.

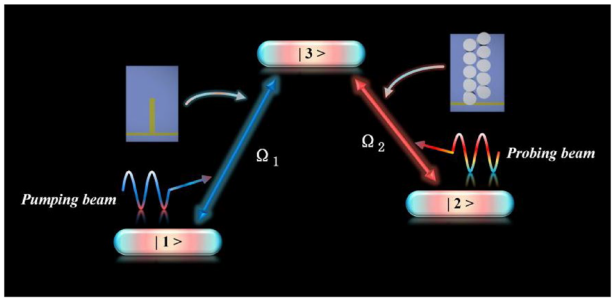

Figure 7. Schematic diagram of EIT in the three-level atomic system.

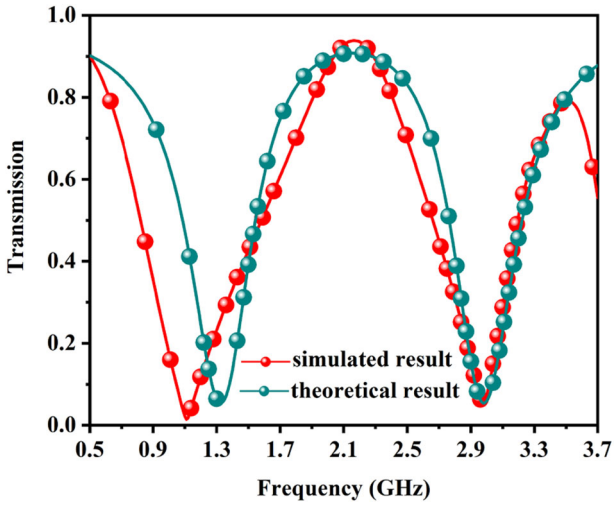

Figure 8. The comparison of simulated and theoretical transmission curves of the structure (The simulation takes into account the loss of FR4).

We fitted the curve by software Matlab and obtained the following fitting parameters: $g = 0.672$, $\gamma_1 = 0.667$, $\gamma_2 = 0.295$, $\Omega = 1.6399$. The curve obtained by fitting Equation (3) and the numerical simulation result can be roughly matched, as shown in **Figure 8**, which shows that the two-oscillator model is valid for the given metamaterial. (The fundamental reason why the two curves do not coincide exactly is that there may be resonance between the dielectric columns.)

4. Parameters Discussion

When the width w of the CW changes, the transmission spectra also change. The transmission spectra for $w = 1.5$, 2.5, 3.5, and 4.5 mm are given, which are illustrated in **Figure 9a**. The transmission peaks of the curves appear at 2.31, 2.21, 2.17, and 2.15 GHz with their values of 0.987, 0.985, 0.983, and 0.979, respectively, when $w = 1.5$, 2.5, 3.5 and 4.5 mm. The values of the transmission peaks do not shift considerably as w increases, but peaks move toward the lower frequency zone. The change in w has little effect on the dips in the low-frequency area. The values of dips in the high-frequency zone are 0.119, 0.051, 0.041, and 0.046 for the w of 1.5, 2.5, 3.5, and 4.5 mm, which occur at 3.15, 3.03, 2.99, 2.96 GHz, respectively. The values of the dips tend to decrease when w increases from 1.5 to 3.5. Comparing the transmission spectra for $w = 3.5$ mm and $w = 4.5$ mm, the two transmission curves almost coincide, and the value of the transmission dip of $w = 3.5$ mm in the high-frequency region is even lower. Therefore, $w = 3.5$ mm is chosen as the width of the CW.

As presented in Figure 9b, the effects of changing the position of the dielectric columns on the transmission spectra are also investigated. The distance that the dielectric columns move along the x-axis in the negative direction is defined as t ($t = 0$ mm is the initial position). The values of the higher frequency dips drop as t increases, while it has little effect on the transmission dips in the low-frequency region. The three spectra, at 2.17, 2.11, and 2.04 GHz, have transmission peaks with values of 0.983, 0.956, and 0.961, respectively, when $t = 0$, 3, and 6 mm. The highest transmission peak is found when $t = 0$ mm, and the frequencies of the peaks decrease with increasing t. In addition, we can see that t mainly changes the fullwidth half maximum (FWHM), and the larger t, the wider the FWHM. The numerical values of FHWM increase from 59.36% to 75.29% when t increase.

The transmission curves shift towards the high-frequency region as the length L of the CW increases that is exhibited in Figure 9c. When $L = 22$, 23, 24, and 25 mm, the transmission peaks occur at 2.33, 2.23, 2.17, and 2.12 GHz with peaks of 0.980, 0.982, 0.983, and 0.983 respectively. The values of the dips in the high-frequency region increase continuously with increasing L, but the dips in low-frequency are more stable. When $L = 24$ mm and $L = 25$ mm, the values of the peaks and dips of the transmission curves do not change much, so the CW with a length L of 24 is selected for the EITM. To investigate the effect of the number of dielectric resonators on the EIT effect, the cases with one dielectric resonator, two dielectric resonators, and five dielectric resonators respectively are discussed. As revealed in Figure 9d, we have discovered that the EIT effect cannot be achieved by too few dielectric resonators or the values of transmission dips of the transmission spectra are high and therefore the EIT transmission is not efficient. High transmission efficiency EIT can only be achieved when the number of resonators is increased to ten.

5. Experimental Section

The sample is produced, and an experiment is conducted to verify the effectiveness of the EITM suggested in this study, and the fabricated prototype is displayed in **Figure 10a**, and the experimental measurement results are presented in Figure 10b. In addition, the simulated and experimental transmission spectra of the EITM are shown in **Figure 11**. Compared to the simulated results, the experimental results show a reduced peak, and the two transmission valleys are slightly shifted toward higher frequencies.

The reasons listed below lead to parasitic capacitance, and these are the main reasons for the drop in the value of peak transmission of the experimental curve.

1) The media substrate obtained by processing may be bent. (2) The upper dielectric columns are not tightly connected to the cut wire and dielectric substrate, which makes air exist between them. (3) When the sample is made, the soldering is not perfect and may lead to poor contact. 4) The double-sided adhesive is used to adhere the dielectric resonators to the FR4 substrate. The bottoms of the dielectric resonators are not attached to the substrate due to the thickness of the double-sided adhesive.

The main reasons for the deviation of the actual experimental frequency points from the theoretically calculated ones are also listed as follows:

(1) The dielectric constants of the experimentally fabricated dielectric resonators have some deviations from those set by theoretical

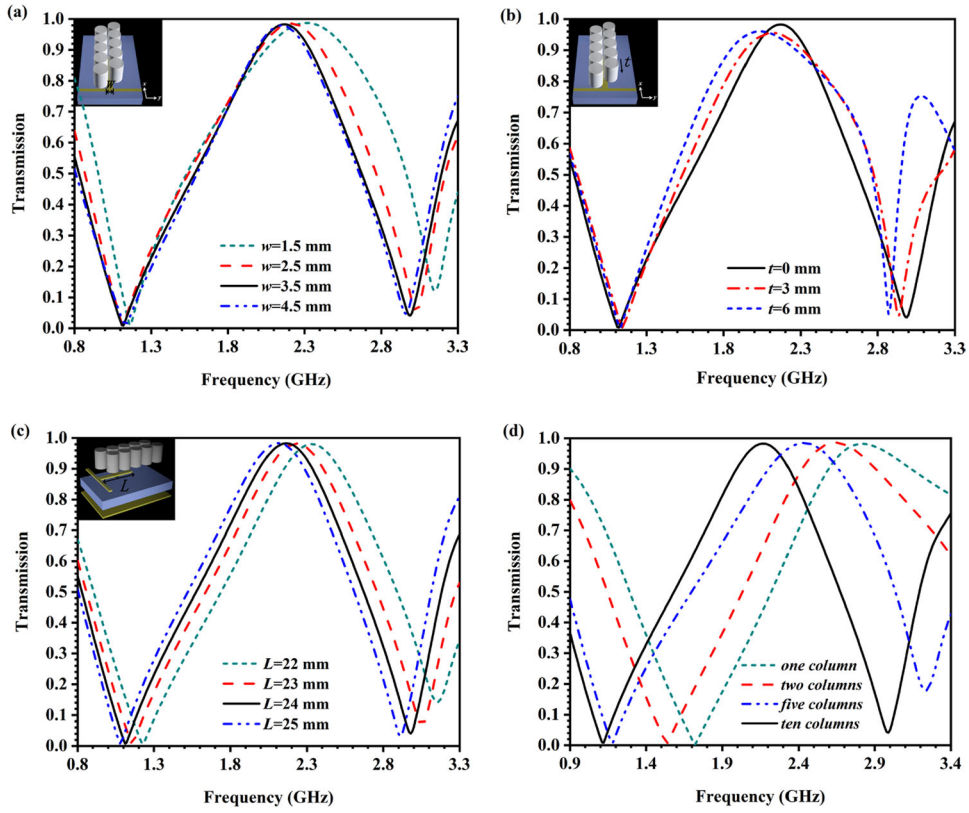

Figure 9. The transmission spectra with different parameters, a) change *w*, b) change *t*, c) change *L*, d) change the number of dielectric resonators.

calculations. (2) Oxidation occurs on metal surfaces which changes the conductivity of the metal.

6. Conclusions

In this paper, a microstrip-line-based dielectric metamaterial consists of the CW and the dielectric columns. As a branch of the microstrip line, the CW is excited directly by the input wave and couples the energy to the dielectric columns that cannot be excited directly by the input wave, resulting in the EIT phenomenon. With a value of 0.983 at 2.17 GHz, this dielectric-based EITM achieves a high transmission peak. Numerical simulation and experimental verification are used to illustrate the effectiveness of the metamaterial. The dielectric-based EITM is extremely efficient, low loss, and easy to fabricate, opening up new possibilities for nonlinear electromagnetic devices, sensors, and electromagnetic switches. The main innovations of this paper are: Unlike traditional EIT metamaterials, we adopt a microstrip line

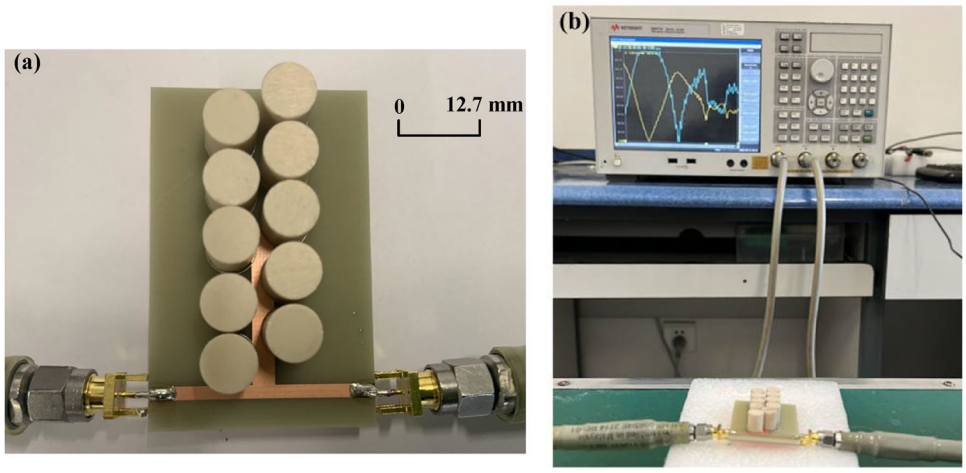

Figure 10. The photograph of the experiment, a) the sample, b) the experimental measurement results.

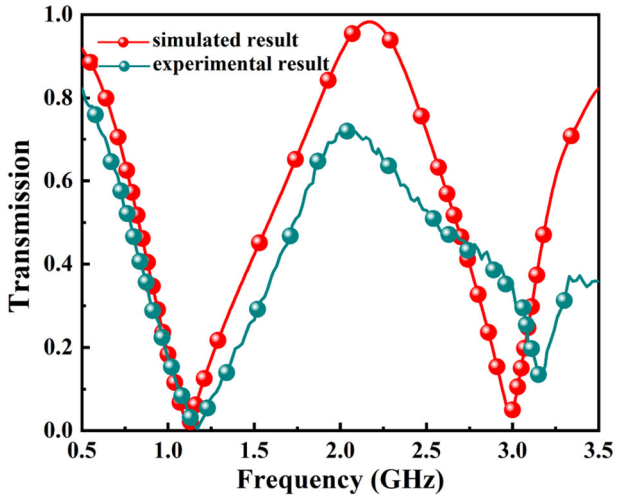

Figure 11. Simulated and experimented transmission spectra of the proposed EITM.

structure and combine metal resonators with dielectric resonators. Overall, the structure combines microstrip line technology and dielectric resonance technology very well.

Conflict of Interest

The authors declare no conflict of interest.

Data Availability Statement

The data that support the findings of this study are available on request from the corresponding author. The data are not publicly available due to privacy or ethical restrictions.

Keywords

dielectric, electromagnetically induced transparency, metamaterials, microstrip line, resonators, two-oscillator model

Received: April 28, 2023
Revised: July 25, 2023
Published online:

[1] L. Jin, J. Zhou, P. Lai, *J. Innov. Opt. Heal Sci.* **2020**, *13*, 3643.
[2] H. Cheng, H. M. Wang, S. S. Zhang, P. P. Xin, J. Luo, H. P. Liu, *Chin. Phys. B* **2017**, *26*, 101.
[3] Y. Kong, J. Cao, W. Qian, C. Liu, S. Wang, *IEEE* **2018**, *10*, 6804410.
[4] R. Li, X. K. Kong, S. B. Liu, Z. M. Liu, Y. M. Li, *Phys. Lett. A* **2019**, *383*, 125947.
[5] S. Hu, D. Liu, H. L. Yang, H. X. Wang, Y. Wang, *Opt. Commun.* **2019**, *450*, 202.
[6] J. Dhanya, A. V. Basiluddeen, R. Ratheesh, *Scr. Mater.* **2017**, *132*, 1.
[7] H. D. Chen, W. J. Feng, Y. Cao, K. Sarabandi, W. Q. Che, *IEEE microwave and wireless components letters: A publication of the IEEE Microwave Theory and Techniques Society* **2017**, *27*, 275.
[8] T. Lei, T. Xiang, J. Wang, R. Zhou, X. Zhu, *Appl. Phys. Express* **2021**, *14*, 067001.
[9] C. Zhu, M. Roman, Y. Zhuang, J. Huang, *Opt. Lett.* **2022**, *47*, 2810.
[10] S. Hu, X. Cheng, W. He, Y. Hu, M. Tong, Z. Xu, *Chin. Opt. Lett.* **2022**, *20*, 113701.
[11] Y. L. Xu, H. X. Li, Y. Y. Wu, L. F. Li, Z. P. Zhan, S. J. Qin, *J. Phys., D. Applied Physics: A Europhysics Journal* **2021**, *54*, 445104.
[12] A. O. Krushynska, M. Miniaci, F. Bosia, N. M. Pugno, *Extreme Mechanics Letters* **2017**, *12*, 30.
[13] H. T. Yudistira, M. Asril, *Micro & Nano Letters* **2021**, *16*, 387.
[14] R. C. Hao, Z. C. Yong, C. Z. Jing, S. M. Xue, *Mod. Phys. Lett. B* **2018**, *32*, 1850332.
[15] Y. Peng, L. V. Besteiro, Y. Huang, W. Jiang, L. Fu, H. H. Tan, C. Jagadish, G. P. Wiederrecht, A. O. Govorov, Z. Wang, *Adv. Opt. Mater.* **2019**, *7*, 1800995.
[16] Y. Zhou, Z. Liang, Z. Qin, X. Shi, X. Wang, *Results in Physics* **2020**, *19*, 103566.
[17] B. X. Wang, Q. Xie, G. X. Dong, W. Q. Huang, *IEEE Photonics Technol. Lett.* **2018**, *30*, 1115.
[18] C. Lao, Y. Liang, X. Wang, H. Fan, F. Wang, H. Meng, J. Guo, H. Liu, Z. Wei, *Nanomaterials* **2019**, *9*, 171.
[19] C. Liu, S. Zha, P. Liu, C. Yang, Q. Zhou, *Appl. Sci.* **2018**, *8*, 2672.
[20] S. Han, H. Yang, L. Guo, *J. Appl. Phys.* **2013**, *114*, 4773.
[21] S. Hu, H. Yang, H. Song, X. Huang, B. Xiao, *J. Appl. Phys.* **2015**, *117*, 4773.
[22] F. Bagci, B. Akaoglu, *J. Appl. Phys.* **2018**, *123*, 173101.1-173101.9.
[23] L. Zhu, J. H. Fu, F. Y. Meng, X. M. Ding, L. Dong, Q. Wu, *IEEE Trans. Magn.* **2014**, *50*, 4000604.
[24] M. Amin, R. Ramzan, O. Siddiqui, *Sci. Rep.* **2018**, *8*, 2357.
[25] N. Muhammad, A. D. Khan, *Plasmonics* **2015**, *10*, 1687.
[26] P. T. Linh, N. Ninh, N. D. Quang, T. T. Lam, B. S. Tung, *Communications in Physics* **2020**, *30*,189.
[27] L. Zhu, Z. Xin, L. Dong, J. Guo, J. H. Xun, M. Y. Zhong, *RSC Adv.* **2018**, *8*, 27342.
[28] X. R. Jin, Y. Lu, J. Park, H. Zheng, G. Feng, Y. P. Lee, J. Y. Rhee, K. W. Kim, H. Cheong, W. H. Jang, *J. Appl. Phys.* **2012**, *111*, 77.
[29] H. Kim, H. Hwang, S. Baek, D. Kim, *Sensors and Actuators, A. Physical* **2018**, *277*, 73.
[30] Y. Sun, H. T. Jiang, Y. P. Yang, Y. W. Zhang, H. Chen, S. Y. Zhu, *Physical review. B, Condensed Matter* **2011**, *83*, 173.
[31] S. Hu, D. Liu, H. L. Yang, *Acta Polym. Sin* **2018**, *47*, 1116001.
[32] L. Zeng, H. F. Zhang, *Ann. Phys.* **2021**, 2100462.
[33] Z. Lei, F. Y. Meng, D. Liang, Q. Wu, B. J. Che, G. Ju, J. H. Fu, Z. Kuang, G. H. Yang, *J. Appl. Phys.* **2015**, *117*, 063901.
[34] X. Fu, J. Wang, Y. Fan, M. Feng, M. Yan, Y. Li, H. Chen, J. Zhang, S. Qu, *Appl. Phys. Lett.* **2018**, *113*,101901.